Title

Molecular imaging of hepatic stellate cell activity by visualization of hepatic integrin αvβ3 expression with SPECT in rat.

Journal

Hepatology (Baltimore, Md.), 54(3)

ISSN

1527-3350

Author

Wu, Jian

Publication Date

2011-05-26

DOI

10.1002/hep.24467

Peer reviewed

Molecular Imaging of Hepatic Stellate Cell Activity by Visualization of Hepatic Integrin $\alpha v\beta 3$ Expression with SPECT in Rat

Feng Li,[1]* Zhengji Song,[1]* Qinghua Li,[1] Jian Wu,[2] Jiyao Wang,[1] Cao Xie,[3] Chuantao Tu,[1] Jian Wang,[1] Xiaowei Huang,[1] and Weiyue Lu[3]

The key factors in the pathogenesis of liver fibrosis are the activation and proliferation of hepatic stellate cells (HSCs), which express integrin $\alpha v\beta 3$ after activation. This study aimed to explore the potential of ^{99m}Tc-labeled cyclic arginine-glycine-aspartic acid pentapeptide (cRGD) as a single photon emission computed tomography (SPECT) radiotracer to image hepatic integrin $\alpha v\beta 3$ expression to reflect HSC activity in fibrotic livers. Rat models of liver fibrosis caused by thioacetamide or carbon tetrachloride (CCl_4) treatment were employed to examine the expression and distribution of integrin $\alpha v\beta 3$ during fibrotic progression or regression. The binding activity of radiolabeled cRGD to integrin $\alpha v\beta 3$ was assessed in liver sections. SPECT was performed to determine hepatic integrin $\alpha v\beta 3$ expression in rats with different stages of liver fibrosis. Protein and messenger RNA (mRNA) levels of integrin αv and $\beta 3$ subunits were increased with the progression of liver fibrosis and reduced with its regression. The cell type that expressed the majority of integrin $\alpha v\beta 3$ in fibrotic livers was found to be activated HSCs. The cRGD binding to activated HSCs displayed a high receptor-coupling affinity and an abundant receptor capacity. Iodine-125 (^{125}I)-labeled cRGD bound to fibrotic liver sections and the binding activity was the highest in advanced fibrosis. Intravenously administered carboxyfluorescein-labeled cRGD was accumulated in fibrotic liver, and the accumulation amount was increased with the progression and reduced with the regression of fibrosis. A SPECT imaging study with ^{99m}Tc-labeled cRGD as a tracer demonstrated that the radioactivity ratio of liver to heart increased progressively along with severity of hepatic fibrosis. Conclusion: Hepatic integrin $\alpha v\beta 3$ expression in fibrotic liver reflects HSC activity and its imaging using ^{99m}Tc-labeled cRGD as a SPECT radiotracer may distinguish different stages of liver fibrosis in rats. (HEPATOLOGY 2011;54:1020-1030)

Liver fibrosis and its endstage cirrhosis are major world health problems arising from chronic liver injury by a variety of etiological factors, including hepatitis B, hepatitis C, alcohol, etc.[1] The prognosis and management of chronic liver disease often depends on the degree of liver fibrosis.[2] To date, liver

Abbreviations: aHSCs, activated hepatic stellate cells; α-SMA, α-smooth muscle actin; BDL, bile duct ligation; CCl_4, carbon tetrachloride; cRGD, cyclic arginine-glycine-aspartic acid peptides; ECM, extracellular matrix; FAM, carboxyfluorescein; HSCs, hepatic stellate cells; ^{125}I, iodine-125; ^{125}I-cRGD, ^{125}I-labeled cRGD; LB, liver biopsy; MRAR, the mean radioactivity ratio of liver to heart; qHSCs, quiescent hepatic stellate cells; TAA, thioacetamide; ^{99m}Tc, technetium-99m; ^{99m}Tc-cRGD ^{99m}Tc-labeled cRGD; SPECT, single photon emission computed tomography.

From the [1]Department of Gastroenterology, Zhongshan Hospital Affiliated to Fudan University, Shanghai, China; [2]Department of Internal Medicine, Division of Gastroenterology & Hepatology, UC Davis Medical Center, Sacramento, CA; and [3]Fudan-Pharmco Targeting Drug Research Center, Fudan University, Shanghai, China.

Received November 21, 2010; Revised May 6, 2011; accepted May 12, 2011.

Supported by the National Natural Science Foundation of China (Grant no. 30770970), the Science and Technology Commission of Shanghai Municipality (Grant no. 064119520), and National Science and Technology Major Project (Grant no. 2009ZX09310-006).

**These authors contributed equally to this study.*

Address reprint requests to: Jiyao Wang, M.D., Professor of Medicine, Department of Gastroenterology, Zhongshan Hospital Affiliated to Fudan University, 180 Fenglin Road, Shanghai 200032, China. E-mail: wang.jiyao@zs-hospital.sh.cn; Fax: +86-21-64432583.

View this article online at wileyonlinelibrary.com.

DOI 10.1002/hep.24467

Potential conflict of interest: Nothing to report.

Additional Supporting Information may be found in the online version of this article.

biopsy (LB) has been the only reliable approach of diagnosing and staging liver fibrosis.[1,3] However, LB is invasive and may cause life-threatening complications; they are rare but do occur.[4] Furthermore, the accuracy of LB for assessing fibrosis also has been controversial because of sampling errors and intra- and interobserver variability that may lead to over- or understaging of fibrotic severity.[5-7] In this regard, various noninvasive approaches have been developed to assess liver fibrosis, including ultrasound-based transient elastography (Fibroscan) that evaluates liver fibrosis by measuring liver stiffness,[8,9] and serum markers of liver fibrosis or more sophisticated algorithms or indices combining the results of panels of markers, such as FibroTest.[2] These approaches not only aid physicians to identify patients with liver fibrosis, but also allow to frequently monitor the disease progression and response to therapeutics in a noninvasive fashion.[1,2] Nevertheless, they display a lower accuracy in detecting earlier stages of fibrosis, although they are valuable in identifying cirrhosis.[2,10]

The key factors in hepatic fibrogenesis are the activation and proliferation of hepatic stellate cells (HSCs).[11] As a result of sustained or repeated liver injury, HSCs undergo a process of activation and transform into myofibroblast-like cells, which are characterized by α-smooth muscle actin (α-SMA) expression, excessive syntheses of extracellular matrix (ECM) proteins, mainly type I and type III collagen, and an accelerated rate of proliferation.[11] Consequently, activated HSCs (aHSCs) contribute largely to the intrahepatic connective tissue expansion during fibrogenesis.[11] Thus, these cells represent an ideal target for visualization of fibrogenic processes and potential antifibrotic therapies.

Integrins comprise a large family of cell surface receptors, which are composed of two subunits, α and β, and each $\alpha\beta$ combination has its own binding specificity and signaling properties.[12] Integrins link the intracellular cytoskeleton with ECM components, thereby playing an important role in cell signaling, cell-to-cell adhesion, apoptosis, and cell-matrix interactions.[12,13] Among various integrins discovered to date, integrin $\alpha v\beta 3$ is the most extensively studied. A common feature of integrins like $\alpha v\beta 3$ is that they bind to ECM proteins by way of the three amino acid sequence of arginine-glycine-aspartic acid (RGD).[12,13] Over the past decade, many radiolabeled cyclic RGD peptides (cRGD) have been developed to be new radiotracers for selectively imaging integrin $\alpha v\beta 3$-positive tumors by positron emission tomography (PET) or single photon emission computed tomography (SPECT).[14-16]

Recently, Patsenker et al.[17] observed that hepatic expression of integrin $\beta 3$ subunit was markedly upregulated in rats with bile duct ligation (BDL) and correlated with the stage of fibrosis. Additionally, it has been demonstrated that integrin $\alpha v\beta 3$ is expressed by HSCs during their activation *in vitro* and that it promotes HSC proliferation and survival.[18] In the present study we further evaluated hepatic integrin $\alpha v\beta 3$ expression and identified the cell type that expressed majority of integrin $\alpha v\beta 3$ at different stages of liver fibrosis in rats, then used radiolabeled cRGD as a SPECT radiotracer to image hepatic integrin $\alpha v\beta 3$ expression in order to develop a noninvasive approach to monitor HSC activity during fibrotic progression.

Materials and Methods

Animals. Eight-week-old inbred male Sprague-Dawley rats (body weight 200 ± 20 g) were obtained from the Laboratory Animal Research Center of Fudan University (Shanghai, China) and fed standard laboratory rat chow on a 12-hour light/dark cycle with free access to water and food. The study was approved by the Institutional Ethical Committee of Animal Experimentation and all experiments were performed strictly according to governmental and international guidelines on animal experimentation.

Synthesis and Radiolabeling of cRGD. cRGD (cyclo[Arg-Gly-Asp-D-Phe-Lys], cRGDfK) was synthesized at the Fudan-Pharmaco Targeting Drug Research Center, Fudan University (Shanghai, China) as described.[19] The synthesis of carboxyfluorescein-labeled cRGD (FAM-cRGD) was carried out by mixing the resin containing the cyclic peptides with preactivated 5-FAM (Sigma-Aldrich, Hong Kong, China) for 3 hours before cleaving.

cRGD was labeled with iodine-125 (^{125}I) by dissolving the peptide (20 μg) into [^{125}I]NaI (37 MBq) (PerkinElmer, Hong Kong, China) in a 1.5-mL polypropylene vial coated with 100 μg of iodogen as described.[20] To label cRGD with technetium-99m (^{99m}Tc), 20 μg of cRGD was added to 1.0 mL of Na[^{99m}TcO4] solution (10 μCi) (Shenke Medicinal, Beijing, China) as described.[14] Analytical reverse-phase high-performance liquid chromatography (RP-HPLC) was performed to examine the purity of cRGD and its derivatives. Electrospray ionization mass spectrometry (ESI-MS) analysis was conducted to examine the molecular weight of final products.

Isolation and Culture of Hepatocyte and HSCs. HSCs and hepatocytes (HCs) were isolated from rats (450-550 g) by two steps of collagenase

digestion.[21] Primary rat HSCs cultured for 3 or 7 days after isolation (referred to as day-3 or day-7 HSCs) and primary HC cultured for 24 hours after isolation were used for further experiments. Human umbilical vein endothelial cells (provided by Chinese Academy of Sciences Shanghai Branch) were used as a control.

Fluorescence Trace of FAM-cRGD in Cells. Day-3 HSCs, day-7 HSCs, and HCs were trypsinized and seeded on plastic dishes (2,000/cm^2), and cultured overnight at 37°C. They were washed with Tris-HCl buffer (20 mmol/L, pH 7.4) and incubated with a solution containing 10 μmol/L FAM-cRGD for 45 minutes at 37°C in the dark, then washed with Tris-HCl buffer at 4°C. Cell nuclei were stained with 6-diamidino-2-phenylindole (DAPI) (1:2,000) and examined with Zeiss FISH (fluorescent *in situ* hybridization) Imager system (Axioskop2 and Axiovert100).

Flow Cytometry Analysis. To assess the binding characteristics of cRGD on HSCs and HC, day-3 HSCs, day-7 HSCs, and HCs were first incubated respectively with a solution of 10 μmol/L cRGD, a solution of 10 μmol/L FAM-cRGD, or a mixed solution containing 10 μmol/L FAM-cRGD and 150 μmol/L cRGD for 45 minutes at 37°C in the dark. After incubation, these cells were washed by centrifugation at 1,776*g* for 15 minutes and analyzed by FACS scan flow cytometry (FACSCalibur) with CellQuest software (BD Biosciences, Franklin Lakes, NJ).

In order to assess the binding efficiency of cRGD at different concentrations and different incubation durations to aHSCs, day-7 HSCs were incubated respectively with FAM-cRGD at concentrations of 0.04, 0.2, 1, 5, 25, and 125 μmol/L for 45 minutes, or with 2 μmol/L FAM-cRGD solution for 15, 30, 45, 60, 75, and 90 minutes at 37°C in the dark. After incubation these cells were washed by centrifugation and analyzed.

Radioligand Binding Analysis. Day-7 HSCs were incubated with ^{125}I-cRGD solutions at different concentrations (100-15,000 pmol/L) in a final volume of 0.5 mL for 3.5 hours at 4°C in the dark. Nonspecific binding was measured in the presence of 100 nmol/L cRGD. Radioactivity in cell pellets was determined with a gamma-counter (Wallac 1470-002, Perkin-Elmer, Finland). Bound ligand was calculated by deduction of the nonspecific radioactivity from the total radioactivity of the ligand. According to the Scatchard plot, the binding constant (Kd) and the maximum binding content (Bmax) of ^{125}I-cRGD were calculated.

Animal Models of Liver Fibrosis. In order to induce liver fibrosis, rats were administered thioacetamide (TAA) (0.2 g/kg) intraperitoneally every Tuesday and Friday. Three weeks or 9 weeks after the treatment, treated rats were used for further experiments (referred to as TAA-3w and TAA-9w rats). Rats treated with sodium chloride served as a control group.

Analyses of Liver Fibrosis. Liver sections were stained with hematoxylin and eosin (H&E) and Sirius red. Extent of liver fibrosis was staged by an experienced histologist who was blind to the treatment protocol according to the Ishak staging criteria.[22] Fibrosis was categorized as mild fibrosis (Ishak score $\leq$2) and advanced fibrosis (Ishak score $\geq$3).[23] For morphometric analysis of liver fibrosis, 10 fields (100×) from each section were randomly selected and recorded. The Sirius red staining (fibrotic) areas were measured using a computer-aided manipulator (KS400, Carl Zeiss Vision, Germany).

In addition, liver hydroxyproline content and serum alanine aminotransferase (ALT) and aspartate aminotransferase (AST) levels were determined using assay kits (JianCheng, Nanjing, China) according to the manufacturer's instructions.

Immunofluorescent Colocalization of Integrin αvβ3 in Various Cell Types of Fibrotic Livers. Immunofluorescent staining was performed to reveal the colocalization of integrin $\alpha v\beta 3$ with α-SMA (aHSCs), albumin (HC), CD31 (vascular endothelial cells), CD68 (macrophages), and CD163 (Kupffer cells) in the liver sections. There is no specific antibody against rat integrin $\alpha v\beta 3$ available. To date, the majority of $\beta 3$ has been shown to bind to αv ($\alpha v\beta 3$) or α_{IIb} ($\alpha_{IIb}\beta 3$), and the latter is a membrane receptor expressed only in cells of megakaryocytic lineage and some tumor cells.[12,24] Hence, evaluating positive immunofluorescent staining of the $\beta 3$ subunit represents the positivity of integrin $\alpha v\beta 3$. Primary antibodies against polyclonal anti-$\beta 3$ integrin (1:200; Chemicon, Billerica, MA), monoclonal anti-SMA (1:400; Chemicon), polyclonal anti-albumin (1:50; AbD Serotec, Oxford, UK), monoclonal anti-CD31 (1:50; AbD Serotec), monoclonal anti-CD68 (1:50; AbD Serotec), and monoclonal anti-CD163 (1:50; AbD Serotec) were used. Secondary antibodies included fluorescein isothiocyanate (FITC)-conjugated IgG (1:200) and Cy3-conjugated IgG (1:200). 0.2% Triton X-100 was used for permeabilization when appropriate. DAPI was used for nuclear counterstaining. Multicolored fluorescent staining of liver sections was analyzed by confocal laser scanning microscopy (Leica Microsystems, Wetzlar, Germany). The fluorescent signals of liver sections were video-digitized and analyzed with a software program that automatically outlined the total stained areas with threshold setting (Photoshop 4.0; Adobe).[25] These

Table 1. Primer Sequences Designed for Quantitative Real-Time PCR Analysis

Gene	Forward Primers	Reverse Primers
αV	GCTGAGCAAGGAGGAAGAAATC	ACAGCCCAAAGTGTGAACATCTC
β3	CTATGGAGACACCTGCGAGAAGT	TTCTTACACTCCACACAGTCCTTCTT
α-SMA	GCTCCATCCTGGCTTCTCTATC	GGGCCAGCTTCGTCATACTC
GAPDH	GGGCAGCCCAGAACATCAT	CCAGTGAGCTTCCCGTTCAG

areas were then quantified with NIH Image 1.62 software and the percentage of the merged yellow color region to the total integrin αvβ3-stained green region in each section was calculated. Ten randomly selected amplifying fields (400×) in each section were assessed.

Quantitative Real-Time Polymerase Chain Reaction (qRT-PCR) Analysis. The hepatic messenger RNA (mRNA) levels of αv, β3 integrin subunits and α-SMA were quantitated using qRT-PCR analysis as described.[26] All PCR primers (Table 1) were designed by Primer Premier 5.0 using published rat gene sequences obtained from the National Center for Biotechnology Information database.

Western Blot Assay. The hepatic protein amount of rat αv, β3 integrin subunits and α-SMA was determined by western blot analysis as described.[18]

Historadioautographic Visualization. The liver sections of TAA-treated or control rats (n = 8 per group) were used to visualize ^{125}I-cRGD binding to livers as described.[27] In brief, the liver sections were incubated in Tris-HCl buffer containing 100 pmol/L ^{125}I-cRGD at 4°C for 24 hours. At the same time, the parallel sections were incubated in the buffer mixed with 100 pmol/L ^{125}I-cRGD and 5 μmol/L cRGD to verify whether the excess cRGD would block the binding of ^{125}I-cRGD in liver sections. After incubation, radioautographic films (Amersham, Buckinghamshire, UK) were exposed to labeled sections. After exposure and developing, the films were scanned with an automatic imaging analyzer and the relative absorbance of hepatic historadioautography was measured. The gray-scale of films represented the binding amount of ^{125}I-cRGD in liver sections.

SPECT Imaging. SPECT imaging was performed in control rats and TAA-treated rats (n = 3 per group). Each animal was administered 6 μCi of ^{99m}Tc-cRGD by way of the penile vein. Animals were placed supine on a SPECT meter (Philips IRIX, Best, Netherlands). Anterior images were acquired 15, 30, and 45 minutes after the injection and stored digitally. Then a computer-aided manipulator discriminated the region of interest in the liver and heart and the radioactivity ratio (counts/pixel) of liver to heart was calculated.

Organ Distribution Studies. A tracer dose (6 μCi) of ^{125}I-cRGD was intravenously administrated to control rats and TAA-treated rats (n = 3 per group). Additionally, 6 μCi ^{125}I-cRGD was also administered simultaneously with excessive unlabeled cRGD (500-fold high dosage of ^{125}I-cRGD) (n = 3 per group). Blood samples were collected by heart puncture 45 minutes after dosage and the organs and tissues were collected, washed in saline, and weighed. Subsequently, radioactivity in the samples was determined by a gamma-counter. The total radioactivity per organ was calculated and corrected for the blood-derived radioactivity. The organ accumulation of ^{125}I-cRGD was calculated as a percentage of the injected dose per gram of wet tissue mass (%ID/g).

Statistical Analysis. All collected data were expressed as mean ± standard deviation (SD). Comparisons between groups were achieved by one-way analysis of variance tests (ANOVA) followed by post-hoc tests with SPSS 11.5 statistical software (Chicago, IL) and $P < 0.05$ was considered statistically significant.

Results

Properties of cRGD and Its Radiolabeled Derivatives. The purity of cRGD and all of its derivatives was above 95%. The molecular weight is 693 for cRGD and 962.01 for FAM-cRGD.

Expression and Distribution of Integrin αvβ3 in Fibrotic Livers. Hepatocyte injury and fibrotic septa formation were observed in the livers of TAA-3w rats and the fibrotic area was 5.8 ± 1.2% (Ishake score 1.8 ± 0.6, representing as mild fibrosis). In the livers of TAA-9w rats, extensive bridging fibrosis in addition to a distortion of liver architecture with pseudo-lobule formation was visible. The fibrotic area was significantly increased to 16.5 ± 3.6% (Ishake score 5.3 ± 0.7, representing as advanced fibrosis) ($P < 0.05$) (Fig. 1A,B). Hydroxyproline content in liver tissue was markedly increased with the progression of liver fibrosis (Fig. 1C). Serum ALT and AST levels in the TAA-3w group was higher than in the control group and the TAA-9w group ($P < 0.05$ for all comparison) (Fig. 1D).

With the progression of liver fibrosis, hepatic mRNA levels and protein levels of αv and β3 integrin subunits and α-SMA were markedly increased and were the highest in rats with advanced fibrosis (Fig. 1E,F).

To colocalize expression of integrin αvβ3 with albumin, α-SMA, CD31, CD68, and CD163, double immunofluorescent staining was performed in the livers

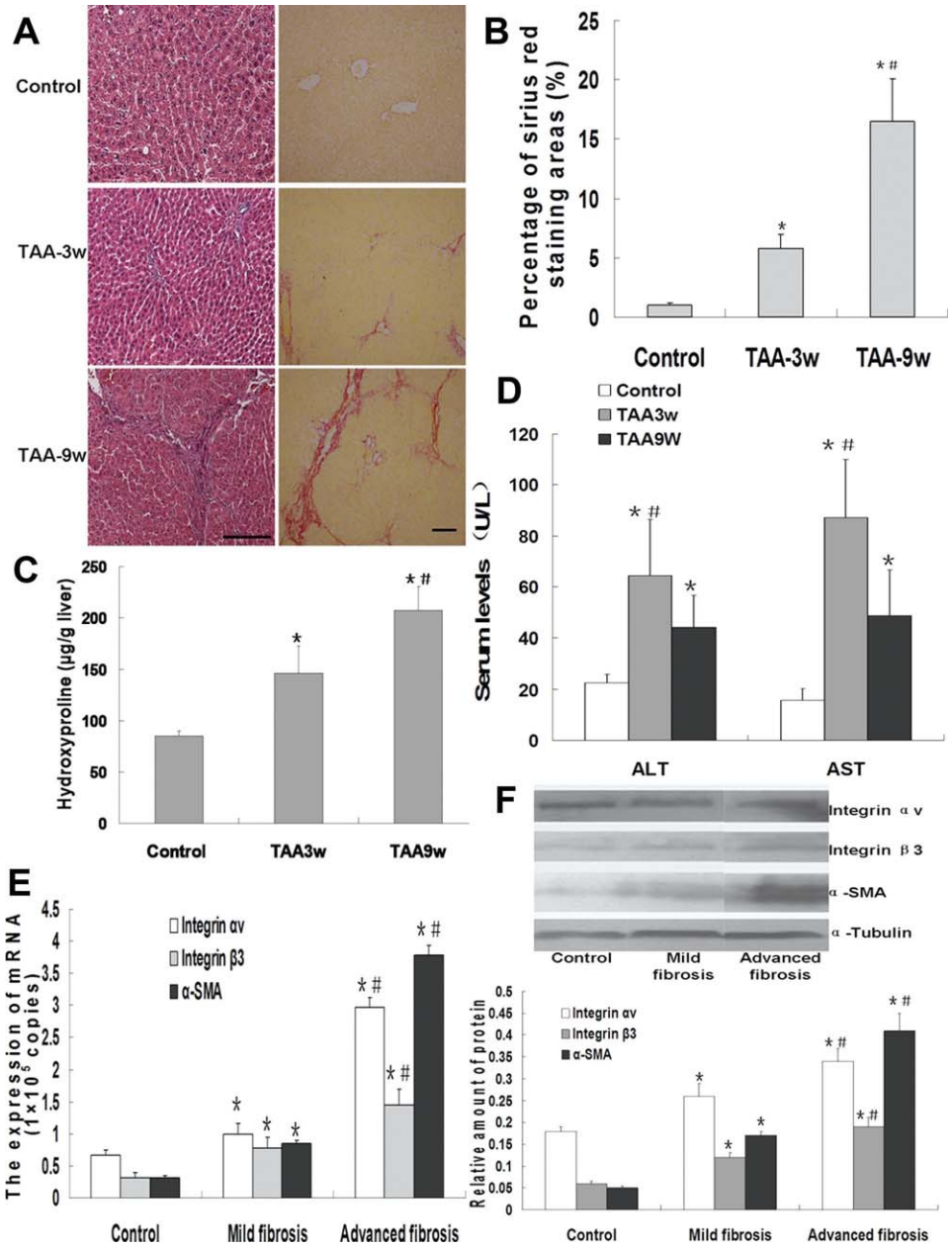

Fig. 1. Expression of integrin $\alpha v\beta 3$ in fibrotic livers treated with TAA. Liver fibrosis was induced in rats by treatment with TAA (0.2 g/kg, intraperitoneal every Tuesday and Friday) for 3 and 9 weeks (referred to as TAA-3w and TAA-9w). The rats treated with 0.9% (v/v) sodium chloride served as a control group. Liver fibrosis was staged according to the Ishak staging criteria. Fibrosis was categorized as mild fibrosis (Ishak score ≤ 2) and advanced fibrosis (Ishak score ≥ 3). (A) Representative micrographs of hepatic histology stained with H&E (left, 200×) and Sirius red (right, 100×). Scale bars = 100 μm. (B) Comparison of the Sirius-red staining (fibrotic) area in TAA-treated and control groups (n = 8 per group). For semiquantitative analysis of liver fibrosis, 10 fields (100×) from each section were randomly selected, recorded, and the Sirius red staining areas were measured. (C) Hydroxyproline content in liver tissue was determined spectrophotometrically and expressed by μg/g liver tissue (n = 8 per group). (D) Serum ALT and AST levels were determined (n = 8 per group). (E) mRNA levels of α-SMA, αv and β3 integrin subunits examined by quantitative real-time RT-PCR analysis in the livers from rats with mild fibrosis and advanced fibrosis induced by TAA treatment for 3 weeks and 9 weeks. Data are expressed as means ± SD (n = 8 per group). (F) Relative protein amounts of α-SMA, αv and β3 integrin subunits examined by western blot assay in the livers from rats with mild fibrosis and advanced fibrosis induced by TAA treatment for 3 weeks and 9 weeks. Protein levels are represented as the ratio to α-tubulin. Data are expressed as means ± SD (n = 8 per group). In all panels, *$P < 0.05$ versus control group; #$P < 0.05$ versus TAA-3w group or mild fibrosis group.

of advanced fibrosis. As shown in Figs. 2, 3, the positive staining of integrin $\alpha v\beta 3$ was mainly overlapped with α-SMA staining (Fig. 2B). The percentage of overlapped areas (yellow) of integrin $\alpha v\beta 3$ staining (green) with α-SMA positive-staining (red) was as high as 69.77 ± 8.41%, which was markedly higher than the overlapped staining with albumin (3.70 ± 1.69%, Fig. 2A), CD31 (17.67 ± 5.20%, Fig. 2C), CD68

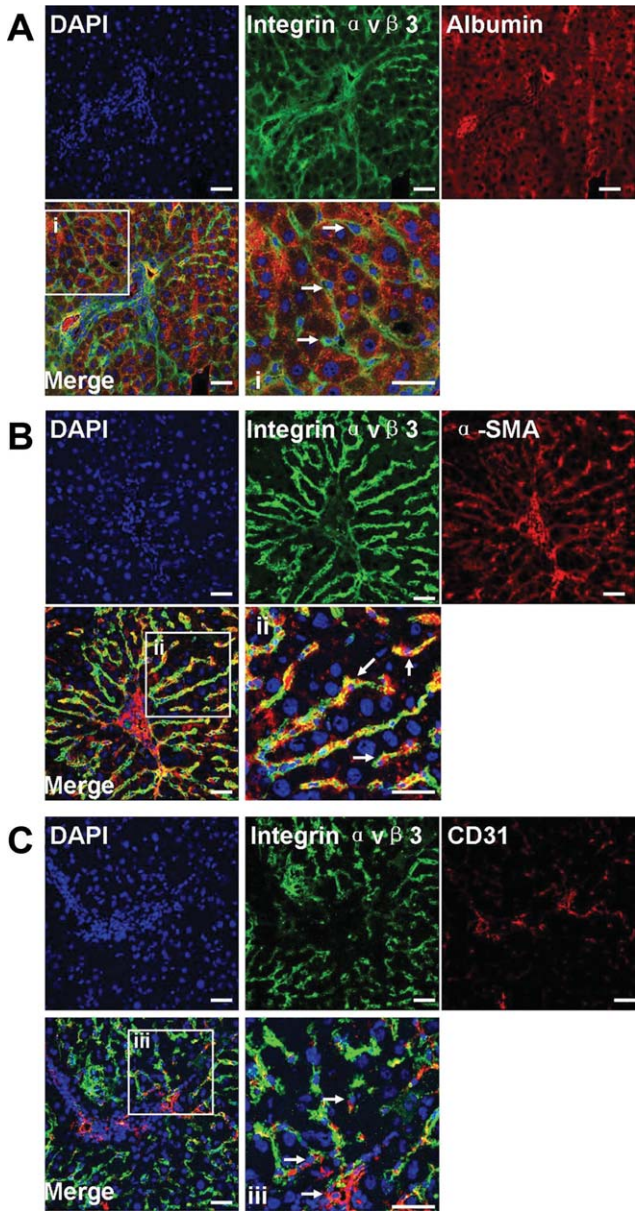

Fig. 2. Immunofluorescent colocalization of integrin $\alpha v\beta 3$ and albumin, α-SMA, or CD31 in fibrotic livers. Albumin (A), α-SMA (B), and CD31 (C) in liver sections from TAA-treated rats with advanced fibrosis were stained with specific first antibodies and visualized by Cy3-conjugated antibody (red). The sections were counterstained with FITC-conjugated anti-integrin $\alpha v\beta 3$ antibody (green) and DAPI (blue) for nuclei staining. The merged images show the yellow color area by overlaying images of the counterstaining. Images were recorded at original magnification (400×), and amplified images (zoom 1:1) corresponding to the indicated areas in boxes are presented in i, ii, and iii. In i, arrows point to the integrin $\alpha v\beta 3$-positive cells and in ii and iii arrows respectively point to the α-SMA- or CD31-positive cells. Scale bars = 100 μm.

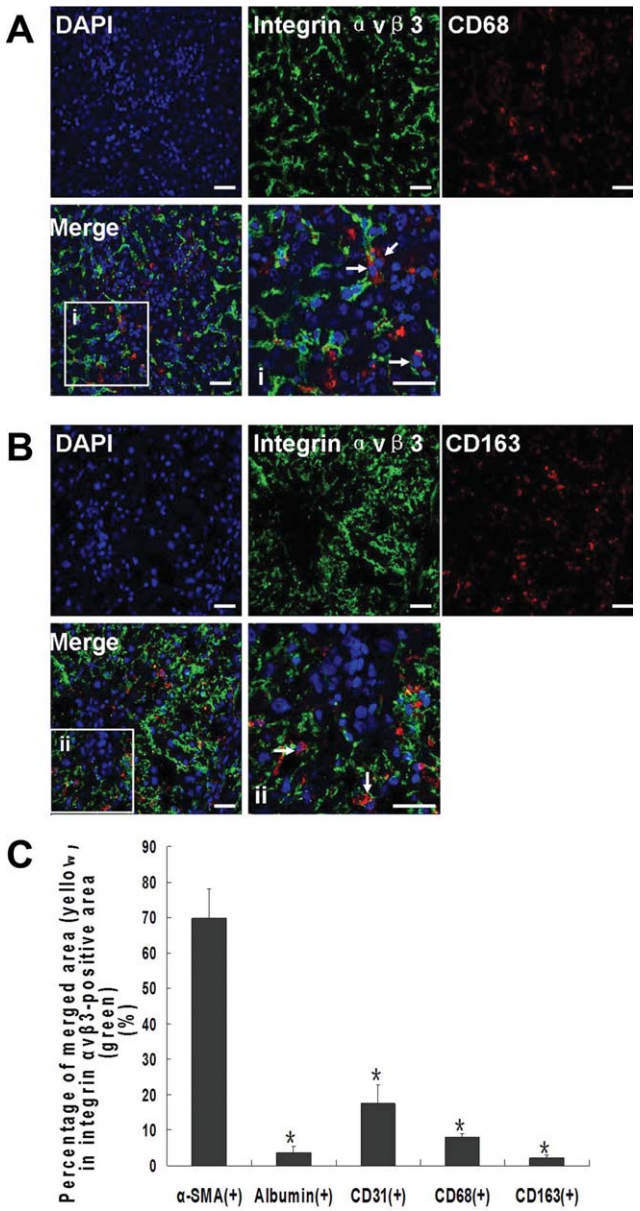

Fig. 3. Immunofluorescent colocalization of integrin $\alpha v\beta 3$ with CD68 or CD163 in fibrotic livers and semiquantitation of the colocalization of integrin $\alpha v\beta 3$ in parenchymal cells and nonparenchymal cells of fibrotic livers. Representative fluorescent images of CD68 (A) and CD163 (B) visualized by Cy3-conjugated antibody (red), counterstained with FITC-conjugated anti-integrin $\alpha v\beta 3$ antibody (green) and DAPI (blue) for nuclei staining from TAA-treated rats with advanced fibrosis. Images were recorded at original magnification (400×) and magnified images (zoom 1:1) corresponding to the indicated areas in boxes are presented in i and ii. Arrows point respectively to the CD68- or CD163-positive cells. Scale bars = 100 μm. (C) The percentage of the merged yellow color area to the positive integrin $\alpha v\beta 3$ staining (green) area. In sections from the same animals integrin $\alpha v\beta 3$ was counterstained with albumin, α-SMA, CD31, CD68, or CD163 separately. The overlapped areas were assessed in 10 randomly selected fields (400×, zoom 1:1) in each liver section from rats with advanced fibrosis (n = 8). Data are expressed in means ± SD. *$P < 0.05$ versus α-SMA-positive cells.

(8.20 ± 0.69%, Fig. 3A), and CD163 (2.10 ± 0.90%, Fig. 3B) ($P < 0.05$ for all comparisons, Fig. 3C). Because α-SMA is thought to be the marker of aHSCs, cardinal cells expressing integrin $\alpha v\beta 3$ in the liver sinusoid areas with advanced fibrosis are considered aHSCs. In livers with mild fibrosis, cardinal cells

expressing integrin $\alpha v\beta 3$ were also found to be aHSCs (data not shown). Therefore, the findings confirm that the majority of integrin $\alpha v\beta 3$ is expressed in aHSCs, and much less $\alpha v\beta 3$ is expressed in parenchymal cells and other nonparenchymal cells.

***Binding Characteristics of cRGD with HSCs* In Vitro.** Day-3 HSCs displayed a quiescent phenotype (qHSCs), and were negative for α-SMA staining. After being cultured for 7 days, HSCs transformed into an activated cell type (aHSCs) and were positive for α-SMA staining (data not shown). The cRGD binding features were characterized as follows.

At first, the binding of FAM-cRGD to qHSCs, aHSCs, and HC was assessed. FAM-cRGD was uptaken by aHSCs, not by qHSCs or HC (Fig. 4A). Fluorescent intensity of qHSCs incubated with 10 μmol/L unlabeled cRGD was higher than that of aHSCs ($P < 0.05$), which indicated that there was higher fluorescent background in qHSCs. However, after being incubated with 10 μmol/L of FAM-cRGD for 45 minutes, the fluorescent intensity of qHSCs did not increase. In contrast, the fluorescent intensity of aHSCs increased up to nearly 3-fold compared to qHSCs. When aHSCs were incubated with the mixed solution containing FAM-cRGD and excess cRGD for 45 minutes, the increase in fluorescent intensity was abrogated in aHSCs (Fig. 4B). There was no marked change in fluorescent intensity of HC after culture with FAM-cRGD.

Second, when aHSCs were incubated with FAM-cRGD in a series of increasing concentrations for 45 minutes their fluorescent intensity was accordingly increased to 1.0 to 11.1-fold. In addition, when aHSCs were incubated with 2 μmol/L of FAM-cRGD for 15 to 90 minutes a 1.3 to 4.5-fold increase in fluorescent intensity was noted accordingly (Fig. 4C).

Lastly, ^{125}I-cRGD was used to further assess the binding characteristics of cRGD with aHSCs. According to the Scatchard plot, the Kd was 4.808×10^{-9} mol/L and Bmax was 2.112×10^{-10} mol/L, which indicated that the binding of synthetic cRGD to aHSCs displayed a high receptor-coupling affinity and that there was an abundant receptor capacity in aHSCs (Fig. 4D).

Historadioautographic Visualization of ^{125}I-cRGD in Liver Sections. Hepatic radioautographic visualization of ^{125}I-cRGD was determined. The hepatic relative densitometry of exposed films from fibrotic rats was significantly higher than that of control rats ($P < 0.05$) and was the highest in rats with advanced fibrosis ($P < 0.05$). When the hepatic sections were incubated with the mixed solution of ^{125}I-cRGD and excess cRGD, the relative hepatic absorbance in control rat liver did not change, whereas it was significantly reduced in fibrotic rats ($P < 0.05$) (Fig. 5).

***SPECT Imaging of ^{99m}Tc-Labeled cRGD* In Vivo.** We further assessed hepatic expression of integrin $\alpha v\beta 3$ in TAA-treated rats and control rats with SPECT imaging. ^{99m}Tc-labeled cRGD was used as a SPECT imaging tracer. After intravenous administration, ^{99m}Tc-labeled cRGD was gradually distributed to organs and tissues. The mean radioactivity ratio of liver to heart (referred to as MRAR) in fibrotic rats and control rats gradually increased over time. Thirty minutes after intravenous administration, MRAR in rats with advanced fibrosis was higher than that in control rats and rats with mild fibrosis ($P < 0.05$), but there was no significant difference between rats with mild fibrosis and control rats ($P = 0.17$). Forty-five minutes after intravenous administration, MRAR in fibrotic rats was significantly higher than that in control rats, and the highest was seen in rats with advanced fibrosis ($P < 0.05$) (Fig. 6).

Organ Distribution of ^{125}I-cRGD. The biodistribution of cRGD was studied in control rats and TAA-treated rats (n = 3 per group) at 45 minutes after ^{125}I-cRGD administration. ^{125}I-cRGD was mainly present in the kidneys and the livers of control rats and TAA-treated rats, and little accumulated in the spleen, heart, lungs, and muscles. The accumulation amount of ^{125}I-cRGD in the livers of fibrotic rats was higher than that in control rats ($P < 0.05$), but there was no significant difference between rats with mild fibrosis and those with advanced fibrosis. In the kidneys of rats with advanced fibrosis, the accumulation amount of ^{125}I-cRGD was lower than that in the other two groups ($P < 0.05$). There was no significant difference in the accumulation amount in other organs and tissues between treated and nontreated rats (Fig. 7A).

After ^{125}I-cRGD was injected simultaneously with excess unlabeled cRGD, the hepatic accumulation amount of ^{125}I-cRGD was reduced in rats with mild fibrosis ($P = 0.059$) and in rats with advanced fibrosis ($P = 0.013$). There was no significant change in the liver of control rats and in other organs and tissues of three groups (Fig. 7B).

Discussion

For the past several years, many high-affinity integrin $\alpha v\beta 3$ antagonists (RGD-containing cyclic peptides and nonpeptide RGD mimetics) have been proposed as targeting biomolecule carriers to deliver the diagnostic "probes" into the integrin $\alpha v\beta 3$-positive tumors.[15,16,24]

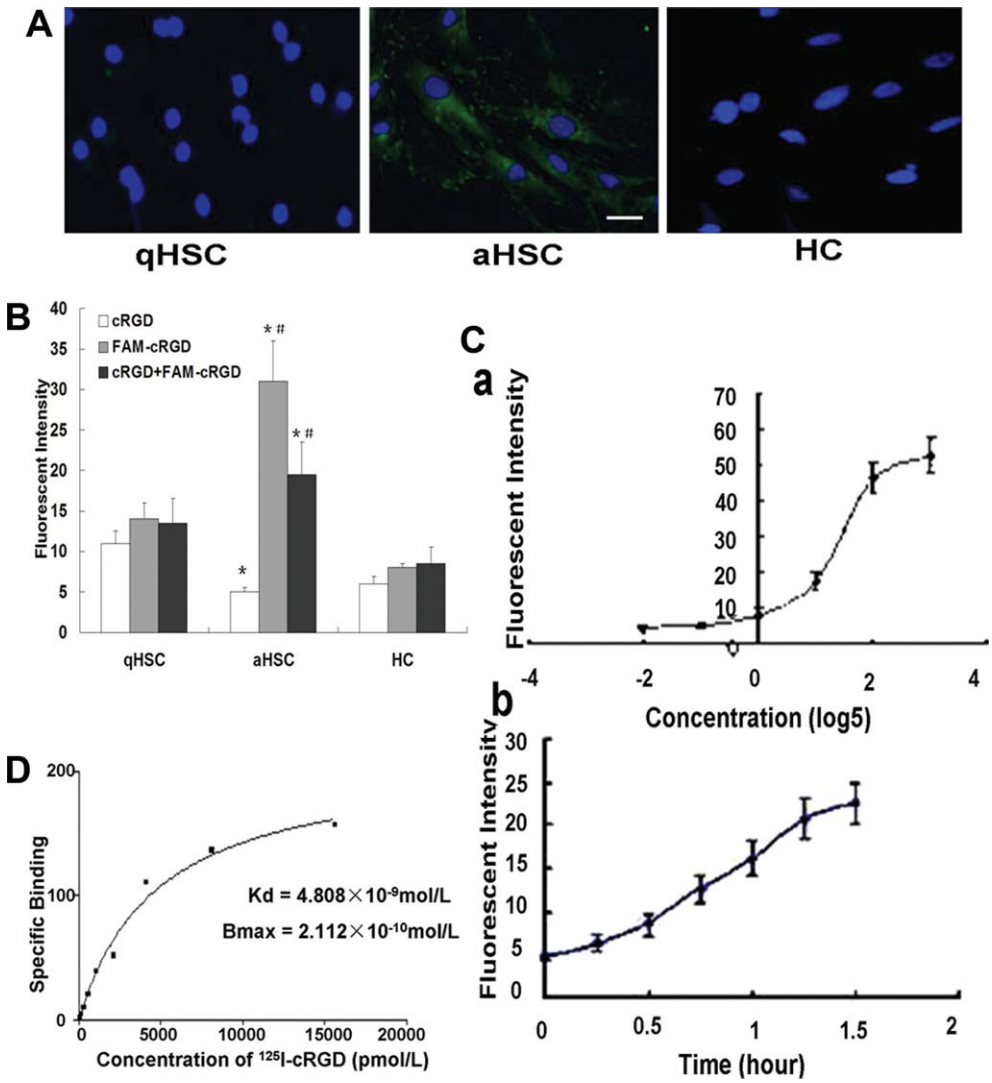

Fig. 4. Binding characteristics of synthetic cRGD with HSCs *in vitro*. Primary rat HSCs cultured for 3 or 7 days after isolation (referred to as day-3 or day-7 HSCs) were used, which represented respectively quiescent or activated HSCs (qHSCs or aHSCs). Primary HCs cultured for 24 hours after isolation were used as controls. (A) Representative fluorescent images of qHSCs, aHSCs, and HC incubated with 10 μmol/L of FAM-cRGD (green) solution for 45 minutes at 37°C in the dark. DAPI (blue) was used to stain the nuclei. Images were taken at original magnification (400×). Scale bars = 100 μm. (B) Day-3 HSC (qHSCs), day-7 HSCs (aHSCs) and HCs were incubated respectively with 10 μmol/L cRGD, 10 μmol/L FAM-cRGD, or the mixed solution containing 10 μmol/L FAM-cRGD and 150 μmol/L cRGD for 45 minutes at 37°C in the dark and were analyzed by flow cytometry. All experiments were undertaken in triplicate. The mean fluorescent intensity in qHSCs, aHSCs, and HC was compared after the incubation. *$P < 0.05$ versus qHSCs; #$P < 0.05$ versus HC. (C) Day-7 HSCs were incubated respectively with the FAM-cRGD solution at concentrations of 0.04, 0.2, 1, 5, 25, and 125 μmol/L for 45 minutes at 37°C in the dark, and the change of the mean fluorescent intensity in HSCs analyzed with flow cytometry is shown (a). In addition, day-7 HSCs were incubated respectively with FAM-cRGD solution (2 μmol/L) for 15, 30, 45, 60, 75, and 90 minutes at 37°C in the dark and the change of the mean fluorescent intensity in HSC is shown (b). All experiments were undertaken in triplicate. (D) Radioligand binding analyses of cRGD with integrin $\alpha v\beta 3$ on day-7 HSCs after incubation with ^{125}I-cRGD solutions at concentrations of 100-15,000 pmol/L for 3.5 hours at 4°C in the dark. The binding constant (Kd) and the maximum binding content (Bmax) of ^{125}I-cRGD were calculated according to the Scatchard plot.

In this study we confirmed that integrin $\alpha v\beta 3$ expression in the fibrotic livers of rats treated with TAA was significantly increased compared to that in the normal livers, and was the most significantly increased in advanced fibrosis. We also determined the hepatic integrin $\alpha v\beta 3$ expression in fibrotic rats induced by BDL (data not shown), which was similar to those reported by Patsenker et al.[17] The pathogenesis of liver fibrosis induced by TAA treatment and BDL treatment is different. The former represents as entire lobular fibrosis, whereas the latter as secondary cholestatic fibrosis.[17] The pathologic feature of liver fibrosis caused by chronic CCl_4 intoxication is similar to TAA, and the findings in the Supporting Information showed a significant increase in hepatic integrin $\alpha v\beta 3$ expression after 8 weeks of CCl_4 intoxication. The findings in three models of rat liver fibrosis

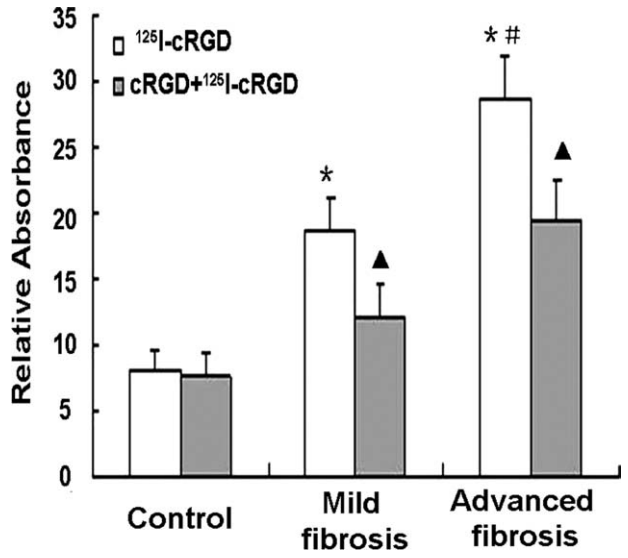

Fig. 5. Historadioautographic images of ^{125}I-cRGD in rat hepatic sections. The hepatic sections from the rats with mild fibrosis and advanced fibrosis induced by TAA treatment for 3 weeks and 9 weeks and the control rats were incubated in the buffer containing 100 pmol/L ^{125}I-cRGD or the buffer mixed with 100 pmol/L ^{125}I-cRGD and 5 μmol/L cRGD. The relative densitometry of the exposed films of hepatic historadioautography is presented. Data represent means ± SD (n = 8 per group). *$P < 0.05$ versus the control group; #$P < 0.05$ versus mild fibrosis group; ▲$P < 0.05$ versus incubated with 100 pmol/L ^{125}I-cRGD.

consistently demonstrated that hepatic integrin $\alpha v\beta 3$ expression is increased along with the development and progression of liver fibrosis. In addition, when liver fibrosis regressed, the hepatic expression level of integrin $\alpha v\beta 3$ was reduced, which was documented in the rat model induced by CCl_4 treatment (Supporting Fig. 1). Thus, these findings provide convincing evidence that hepatic integrin $\alpha v\beta 3$ expression correlated well with the degree of liver fibrosis. In the present study, serum ALT and AST levels, which were used to reflect hepatic inflammation, were not correlated with hepatic integrin $\alpha v\beta 3$ expression in models of liver fibrosis induced by either TAA or CCl_4 treatment.

In addition to HSCs and some tumor cells, integrin $\alpha v\beta 3$ was reported to be expressed in endothelial cells and inflammatory cells, especially monocytes and macrophages.[28-30] In the present study we demonstrated that positive integrin $\alpha v\beta 3$ staining in fibrotic livers was essentially overlapped with positive α-SMA staining, an indicator of aHSCs. By comparing the percentage of overlapped integrin $\alpha v\beta 3$ staining with markers of various cell types in the liver, integrin $\alpha v\beta 3$ expressed in parenchymal cells and other nonparenchymal cells was shown to be significantly lower than that in α-SMA-positive cells, which was as high as ≈70%. Thus, we conclude that the major cell type expressing integrin $\alpha v\beta 3$ in fibrotic livers is aHSCs. Hepatic α-SMA expression was found to be increased or reduced with the progression or regression of fibrosis, which correlates well with the degree of liver fibrosis and expression of integrin $\alpha v\beta 3$. In this context, it is convincing that the visualization of hepatic integrin $\alpha v\beta 3$ expression reflects the activity of aHSCs, which represent an ideal target for monitoring fibrogenic process.

After culturing with FAM-cRGD, aHSCs, but not qHSCs or HC, took up FAM-cRGD, and the uptake rate was partially inhibited by excess unlabeled cRGD. These findings indicate that the synthetic cRGD, which specifically binds to integrin $\alpha v\beta 3$ receptors, was taken up largely by aHSCs. In addition, the binding of FAM-cRGD to aHSCs was increased along with prolonged culture duration and with an increased concentration of FAM-cRGD, which implies that the

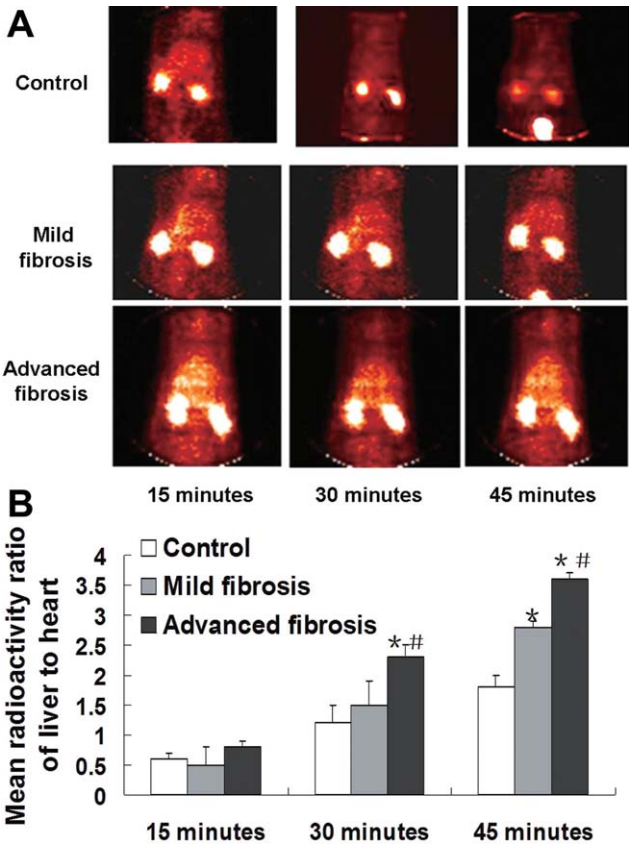

Fig. 6. SPECT images of the integrin $\alpha v\beta 3$ expression in livers of the normal control rats and the rats with liver fibrosis. Mild and advanced fibrosis was respectively induced in rats by TAA-treatment for 3 weeks and 9 weeks. Each animal was administered 6 μCi of ^{99m}Tc-cRGD by way of the penile vein. (A) The representative SPECT images were obtained at 15, 30, and 45 minutes after administration. (B) The region of interest (ROI) in the liver and heart was discriminated and the radioactivity (counts/pixel) ratio of liver to heart was calculated and compared. Data represent means ± SD (n = 3 per group). *$P < 0.05$ versus the control group; #$P < 0.05$ versus mild fibrosis.

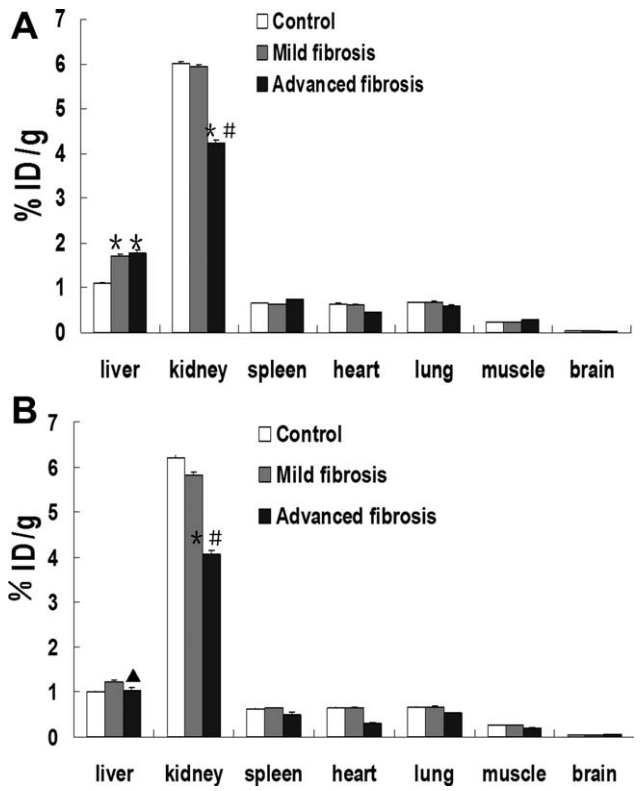

Fig. 7. Organ biodistribution of ^{125}I-cRGD in rats. The rats with mild fibrosis and advanced fibrosis and normal rats received a single intravenous injection of 6 μCi ^{125}I-cRGD (A) or 6 μCi ^{125}I-cRGD simultaneously with excess unlabeled cRGD (500-fold high dosage of ^{125}I-cRGD) (B) by way of the penile vein. Organ biodistribution was analyzed at 45 minutes after injection. The organ accumulation amount of ^{125}I-cRGD was calculated as a percentage of the injected dose per gram of wet tissue mass (%ID/g). Data represent means $\pm$ SD (n = 3 per group). *$P < 0.05$ versus the control group; #$P < 0.05$ versus mild fibrosis; ▲$P < 0.05$ versus injected with 6 μCi ^{125}I-cRGD.

binding was time-dependent and concentration-dependent. Our radioligand binding assay further demonstrated that the binding of synthetic cRGD to aHSCs displayed a high receptor-coupling affinity and an abundant receptor capacity. After incubation with ^{125}I-cRGD, there was more ^{125}I-cRGD accumulation in fresh hepatic sections from fibrotic rats than those from the control rats, and the sections from rats with advanced fibrosis had the highest coupling activity. Excess unlabeled cRGD did not block the accumulation of ^{125}I-cRGD in the sections from the normal control rats, but significantly reduced the accumulation in the sections from the fibrotic rats. More important, after intravenous injection FAM-cRGD was found to accumulate in fibrotic livers and the accumulation amount was increased with the progression of liver fibrosis and reduced with the regression of liver fibrosis (Supporting Fig. 2). Taken together, these results provide convincing evidence that visualizing hepatic expression of integrin $\alpha v\beta 3$ could distinguish HSC activity in different stages of liver fibrosis.

In the organ distribution study of ^{125}I-cRGD, we found that the predominant excretion pathway of synthetic cRGD was through kidneys and hepatobiliary routes in both control and fibrotic rats, and that there was minimal accumulation in other organs 45 minutes after intravenous administration, indicating that the *in vivo* retention of radionuclide was minimal. The hepatic accumulation of ^{125}I-cRGD in rats with liver fibrosis was higher than that in control rats and administration of excessive unlabeled cRGD reduced ^{125}I-cRGD accumulation in fibrotic livers, especially in advanced fibrosis, which indicated that the accumulation of ^{125}I-cRGD in fibrotic liver was interfered by competing for the receptors with unlabeled cRGD.

Given the fact that synthesized cRGD was mainly excreted through the renal and hepatobiliary routes, the image of ^{99m}Tc-labeled cRGD in livers by SPECT modality would inevitably be interfered by the shadow of the kidneys, especially the right kidney neighboring the liver. In normal rats, the highest basal expression of $\beta 3$ integrin mRNA was found in liver and less was found in heart.[17] In our biodistribution study, accumulation of ^{125}I-cRGD in the heart did not change markedly in fibrotic rats compared to control rats. Therefore, the accumulation of cRGD in the heart was relatively invariant in fibrotic rats in comparison to control rats, and MRAR could be considered a valuable index to reflect the relative binding amount of ^{99m}Tc-labeled cRGD in the liver. MRAR was significantly increased in rats with liver fibrosis compared to that in control rats. It was the highest in the rats with advanced fibrosis, whereas the biodistribution study showed that there was the least ^{125}I-cRGD accumulation in the kidneys from these rats with advanced fibrosis. Furthermore, in the organ distribution study it was evident that there was no significant difference in ^{125}I-cRGD accumulation in kidneys between the rats with mild fibrosis and the control rats, whereas MRAR in the mild fibrosis was significantly higher than that in normal livers. Based on these findings, we overcame the disturbance of renal visualization to hepatic visualization in imaging integrin $\alpha v\beta 3$ expression with SPECT imaging by comparing MRAR in rats, although further studies are needed to further improve this imaging modality.

In conclusion, the findings in the present study demonstrate that enhanced expression of integrin $\alpha v\beta 3$ in fibrotic liver reflects the activity of activated HSCs and that the expression levels correlate with fibrotic progression and regression. SPECT imaging using

^{99m}Tc-labeled cRGD as a radiotracer may noninvasively distinguish different stages of liver fibrosis, which implicates a potential value in monitoring HSC activity by imaging hepatic integrin $\alpha v\beta 3$ expression.

References

1. Rockey DC, Caldwell SH, Goodman ZD, Nelson RC, Smith AD. American Association for the Study of Liver Diseases. Liver biopsy. Hepatology 2009;49:1017-1044.
2. Castéra L, Vergniol J, Foucher J, Le Bail B, Chanteloup E, Haaser M, et al. Prospective comparison of transient elastography, Fibrotest, APRI, and liver biopsy for the assessment of fibrosis in chronic hepatitis C. Gastroenterology 2005;128:343-350.
3. Dienstag JL. The role of liver biopsy in chronic hepatitis C. Hepatology 2002;36:S152-S160.
4. Cadranel JF, Rufat P, Degos F. Practices of liver biopsy in France: results of a prospective nationwide survey. For the Group of Epidemiology of the French Association for the Study of the Liver (AFEF). Hepatology 2000;32:477-481.
5. Regev A, Berho M, Jeffers LJ, Milikowski C, Molina EG, Pyrsopoulos NT, et al. Sampling error and intraobserver variation in liver biopsy in patients with chronic HCV infection. Am J Gastroenterol 2002;97:2614-2618.
6. Colloredo G, Guido M, Sonzogni A, Leandro G. Impact of liver biopsy size on histological evaluation of chronic viral hepatitis: the smaller the sample, the milder the disease. J Hepatol 2003;39:239-244.
7. Bedossa P, Dargère D, Paradise V. Sampling variability of liver fibrosis in chronic hepatitis C. Hepatology 2003;38:1449-1457.
8. Nguyen-Khac E, Chatelain D, Tramier B, Decrombecque C, Robert B, Joly JP, et al. Assessment of asymptomatic liver fibrosis in alcoholic patients using fibroscan: prospective comparison with seven non-invasive laboratory tests. Aliment Pharmacol Ther 2008;28:1188-1198.
9. Sandrin L, Fourquet B, Hasquenoph JM, Yon S, Fournier C, Mal F, et al. Transient elastography: a new noninvasive method for assessment of hepatic fibrosis. Ultrasound Med Biol 2003;29:1705-1713.
10. Shaheen AA, Wan AF, Myers RP. FibroTest and FibroScan for the prediction of hepatitis C-related fibrosis: a systematic review of diagnostic test accuracy. Am J Gastroenterol 2007;102:2589-2600.
11. Friedman SL. Liver fibrosis—from bench to bedside. J Hepatol 2003; 38:S38-S53.
12. Giancotti FG, Ruoslahti E. Integrin signaling. Science 1999,285: 1028-1032.
13. Beer AJ, Schwaiger M. Imaging of integrin αvβ3 expression. Cancer Metastasis Rev 2008;27:631-644.
14. Shi J, Wang L, Kim YS, Zhai S, Liu Z, Chen X, Liu S. Improving tumor uptake and excretion kinetics of 99mTc-labeled cyclic arginine-glycine-aspartic (RGD) dimmers with triglycine linkers. J Med Chem 2008;51:7980-7990.
15. Costouros NG, Diehn FE, Libutti SK. Molecular imaging of tumor angiogenesis. J Cell Biochem 2002;39:S72-S78.
16. Haubner R, Wester HJ. Radiolabeled tracers for imaging of tumor angiogenesis and evaluation of anti-angiogenic therapies. Curr Pharm Des 2004;10:1439-1455.
17. Patsenker E, Popov Y, Stickel F, Schneider V, Ledermann M, Sgesser H. Pharmacological inhibition of integrin αvβ3 aggravates experimental liver fibrosis and suppresses hepatic angiogenesis. Hepatology 2009;50: 1501-1511.
18. Zhou X, Murphy FR, Gehdu N, Zhang J, Iredale JP, Benyon RC. Engagement of integrin αvβ3 regulates proliferation and apoptosis of hepatic stellate cells. J Biol Chem 2004;279:23996-24006.
19. Haubner R, Wester HJ, Reuning U, Senekowitsch-Schmidtke R, Diefenbach B, Kessler H, et al. Radiolabeled alpha(v)beta3 integrin antagonists: a new class of tracers for tumor targeting. J Nucl Med 1999;40: 1061-1071.
20. Kuijpers BH, Groothuys S, Soede AC, Laverman P, Boerman OC, van Delft FL, et al. Preparation and evaluation of glycosylated arginine-glycine-aspartate (RGD) derivatives for integrin targeting. Bioconjug Chem 2007,18:1847-1854.
21. Zhu J, Wu J, Frizell E, Liu SL, Bashey R, Rubin R, et al. Rapamycin inhibits hepatic stellate cell proliferation in vitro and limits fibrogenesis in an in vivo model of liver fibrosis. Gastroenterology 1999;117: 1198-1204.
22. Ishak K, Baptista A, Bianchi L, Callea F, De Groote J, Gudat F, et al. Histological grading and staging of chronic hepatitis. J Hepatol 1995; 22:696-699.
23. Bodini S, Kallman J, Wheeler A, Prakash S, Gramlich T, Jondle DM, et al. Impact of non-alcoholic fatty liver disease on chronic hepatitis B. Liver Int 2007:606-611.
24. Chen YQ, Trikha M, Gao X, Bazaz R, Porter AT, Timar J, et al. Ectopic expression of platelet integrin alphaIIb beta3 in tumor cells from various species and histological origin. Int J Cancer 1997;72: 642-648.
25. Sato Y, Murase K, Kato J, Kobune M, Sato T, Kawano Y, et al. Resolution of liver cirrhosis using vitamin A-coupled liposomes to deliver siRNA against a collagen-specific chaperone. Nat Biotechnol 2008;26: 431-42.
26. Fiorucci S, Antonelli E, Rizzo G, Renga B, Mencarelli A, Riccardi L, et al. The nuclear receptor SHP mediates inhibition of hepatic stellate cells by FXR and protects against liver fibrosis. Gastroenterology 2004; 14:1444-1456.
27. Jia B, Shi JY, Yang Z, Xu B, Liu Z, Zhao H, et al. 99mTc-labeled cyclic RGDfK dimer: initial evaluation for SPECT imaging of glioma integrin alphavbeta3 expression. Bioconjug Chem 2006;17:1069-1076.
28. Hood JD, Cheresh DA. Role of integrins in cell invasion and migration. Nat Rev Cancer 2002;2:91-100.
29. Patsenker E, Popov Y, Wiesner M, Goodman SL, Schuppan D. Pharmacological inhibition of the vitronectin receptor abrogates PDGF-BB-induced hepatic stellate cell migration and activation in vitro. J Hepatol 2007;46:878-887.
30. Chung AS, Gao Q, Kao WJ. Either integrin subunit beta1 or beta3 is involved in mediating monocyte adhesion, IL-1beta protein and mRNA expression in response to surfaces functionalized with fibronectin-derived peptides. J Biomater Sci Polym Ed 2007;18:713-729.